SCIENTIFIC REPORTS

OPEN

Dependence of spin-orbit torque effective fields on magnetization uniformity in Ta/Co/Pt structure

Received: 7 March 2019
Accepted: 25 June 2019
Published online: 25 July 2019

Feilong Luo[1], Qi Ying Wong[1], Sihua Li[1], Funan Tan[1], Gerard Joseph Lim[1], Xuan Wang[1,2] & Wen Siang Lew[1]

The spin-orbit torque (SOT) effective fields, namely field-like and damping-like terms, depend on the thicknesses of heavy metal (HM) and ferromagnetic metal (FM) layers, in a stack comprising of HM/FM/HM or oxide. In this work, we report on the dependence of the SOT effective fields on the magnetization uniformity in the wires comprising of Ta/Co/Pt layer structure. SOT dependence on magnetization uniformity dependence was investigated by concurrent variation of the magnetization uniformity in Co layer and characterization of the SOT effective fields in each wire which excludes the layer thickness dependence influences. Our experimental results reveal that the field-like term decreases while the damping-like term increases with increasing Co magnetization uniformity. The magnetization uniformity influence on the effective fields is attributed to the spin Hall effect, which contributes to the SOT.

The control of magnetization switching in magnetic structures by an electric current is crucial for the development of spintronics devices[1]. An established approach is *via* spin-transfer torque (STT) which involves the transfer of angular momentum from spin-polarized current to the magnetization[2]. Lately, current-induced spin-orbit torque (SOT) has emerged as an efficient alternative to STT[3,4]. The SOT is observed in magnetic multilayer structures composed of a ferromagnetic (FM) layer sandwiched by two heavy metal (HM) layers[5–7]. In this structure, the conduction electrons of FM and HMs exhibit strong spin-orbit coupling which leads to two well-known phenomena, *i.e.*, the Rashba effect and the spin Hall effect (SHE)[3,4]. Due to the Rashba effect, spins accumulate in the FM layer, which exerts both a damping-like and field-like torque on the magnetization of FM layer[8]. Meanwhile, due to SHE, polarized spins are induced to accumulate at the FM/HM interface and diffuse into FM layer, which gives rise to an STT effect on the magnetization[9]. The torque from the Rashba effect and SHE is namely the SOT comprising of a field-like torque and damping-like torque. Generally, the two torques are represented by the two corresponding effective fields, field-like term H_F and damping-like term H_D[3–7,9,10].

The dependence of the two effective fields on the orientation of the magnetization has been studied, especially in materials with perpendicular magnetic anisotropy (PMA)[11–17]. Reported SOT measurements on Ta/CoFeB/MgO structures have shown that the damping-like term H_D changed the direction when the magnetization is reversed[12]. Recently, the dependence of the field-like term H_F which has been considered as a constant on the polar angle of magnetization was observed experimentally in films with PMA[14,15]. The SOT effective fields also depend on the thicknesses of the FM and HM layers in Ta/CoFeB/MgO structure[18]. The increase of both field-like and damping-like terms with respect to the thickness of Ta has been reported, which is due to a more significant amount of current in a thicker Ta layer. For the dependence on the thickness of the FM layer, the field-like term decreases with increasing CoFeB thickness, while the damping-like term remains constant. Such dependence was ascribed to the giant magnetoresistance effect[18]. In the investigations of the referred dependences, sweeping magnetic fields were used. However, the sweeping behavior, *i.e.*, magnetizing process, gives rise to magnetization variation or magnetization non-uniformity in magnetic devices. Hence, to precisely characterize the dependencies, the relationship between the SOT effective fields and the magnetic uniformity is required. Specifically, this relationship in a magnetic system with in-plane magnetic anisotropy (IMA) requires investigation, as the SOT devices based on IMA show promising application in spintronics[19].

Here, we demonstrate the dependence of the SOT effective fields on the magnetization uniformity in wires consisting of Ta/Co/Pt layers with IMA. The impact of HM and FM layers thickness dependence of SOT is

[1]School of Physical and Mathematical Sciences, Nanyang Technological University, 21 Nanyang Link, Singapore, 637371, Singapore. [2]Department of Physics, School of Science, Lanzhou University of Technology, Lanzhou, 730050, PR China. Correspondence and requests for materials should be addressed to W.S.L. (email: wensiang@ntu.edu.sg)

eliminated. Varying the uniformity and characterizing the SOT effective fields were achieved concurrently in each wire by applying a magnetic field along the long axis of the wire. Experimental results show that the field-like term decreases with respect to the magnetization uniformity, whereas the damping-like term increases. It is proposed that the magnetization uniformity increase leads to an increase of electron diffusion constant to decrease the field-like term and increase damping-like term.

Experiments and Discussion

Harmonic Hall resistance measurement technique, which has been reported earlier[20], were employed to characterize the SOT effective fields. In this technique, a constant field, $H_{x-\mathrm{ext}}$, is applied longitudinally to the wire long axis to ensure a constant magnetization uniformity, while a transverse field to the wire, $H_{y-\mathrm{ext}}$, is swept in the plane to obtain the SOT effective fields accurately. The transverse field changes the magnetization azimuthal angle φ_0. With $H_{x-\mathrm{ext}}$ being constant, the cosine of the angle, X, which can be simultaneously calculated by $X = \cos\varphi_0 = H_{x-\mathrm{ext}}/\sqrt{H_{x-\mathrm{ext}}^2 + H_{y-\mathrm{ext}}^2}$. X is used to apply in the expression of the second harmonic Hall resistance $R_{2\mathrm{ndHall}}$ which is:

$$R_{2\mathrm{nd\ Hall}} = \frac{R_{\mathrm{AHE}}}{2H_{\perp}} H_{\mathrm{D}} X + \frac{R_{\mathrm{PHE}}}{H_{x-\mathrm{ext}}} H_{\mathrm{F}}(2X^4 - X^2), \tag{1}$$

where H_D and H_F are the damping-like term and field-like term, respectively, R_{AHE} and R_{PHE} are the amplitudes of anomalous Hall effect and planar Hall effect resistances, and $H_{\perp}$ is the effective field orientating the magnetization in the film plane. By fitting the experimental second harmonic Hall resistance with Eq. (1), the SOT effective fields can be extracted. In Eq. (1), the parameter $R_{\mathrm{PHE}}/H_{x-\mathrm{ext}}$ can be obtained from the first harmonic Hall resistance $R_{1\mathrm{st\ Hall}}$, which is expressed as $R_{1st\ \ Hall} = R_{PHE} \sin 2\varphi_0$. Due to the expression of $\cos\varphi_0$, the maximum and minimum values of $R_{1\mathrm{st\ Hall}}$ occur at $H_{y-\mathrm{ext}} = \pm H_{x-\mathrm{ext}}$, which give R_{PHE}.

The measurements were carried out in the wires with stacks of Ta(t nm)/Co(2 nm)/Pt(5 nm), where $t = 4, 6, 8$ and 10[20]. The fabrication and patterning processes of the wires are described elsewhere[17,20–22]. The SOT fields are quantified as a function of the longitudinal fields in the sample of Ta(4 nm)/Co(2 nm)/Pt(5 nm)[20]. In this quantification, the constant longitudinal field $H_{x-\mathrm{ext}}$ was applied in a range of 250 Oe to 650 Oe with a 50 Oe increment. For each value of $H_{x-\mathrm{ext}}$, the ratio of the maximum value of the sweeping field $H_{y-\mathrm{ext}}$ to $H_{x-\mathrm{ext}}$ was fixed. An AC frequency of 307.1 Hz was used for the low-frequency harmonic Hall resistance measurements. The amplitudes of the AC current were in the range of 3×10^{10}~10×10^{10} Am^{-2} with an increment of 10^{10} Am^{-2}. The first and second harmonic Hall resistances were measured using a 7265 DSP lock-in amplifier. The obtained harmonic Hall resistances at applied fields $H_{x-\mathrm{ext}} = 250$ Oe, 450 Oe, and 650 Oe and current density of 1×10^{11} Am^{-2} are shown in Fig. 1.

The measured first harmonic Hall resistances $R_{1\mathrm{st\ Hall}}$ exhibit typical $\sin 2\varphi_0$ behaviors as functions of the azimuthal angle φ_0 of the magnetization, and the minimum and maximum values of $R_{1\mathrm{st\ Hall}}$ are at $\varphi_0 = \pm 45$ degrees. Correspondingly, for each value of $H_{x-\mathrm{ext}}$ shown in the inset of Fig. 1(a), the minimum and maximum values of $R_{1\mathrm{st\ Hall}}$ occur at $H_{x-\mathrm{ext}} = \pm H_{y-\mathrm{ext}}$, which give the values of R_{PHE} and the ratio of $R_{\mathrm{PHE}}/H_{x-\mathrm{ext}}$ shown in Fig. 1(b). In Fig. 1(c), the measured second harmonic Hall resistances, $R_{2\mathrm{nd\ Hall}}$, are shown to increase with increasing X for each value of $H_{x-\mathrm{ext}}$. Fitting the experimental $R_{2\mathrm{nd\ Hall}}$ by Eq. (1), where the values of R_{PHE} and $R_{\mathrm{PHE}}/H_{x-\mathrm{ext}}$ are recorded in Fig. 1(b), we compute the two effective SOT fields, H_{F} and H_{D}.

As shown in Fig. 2, for each value of $H_{x-\mathrm{ext}}$, H_{F} and H_{D} increase with respect to the current density at each value of $H_{x-\mathrm{ext}}$. The values of H_{F} and H_{D} are similar to that reported in the same stack[20]. We notice that H_{F} and H_{D} vary with the longitudinal field for each value of the applied current densities. However, at the current density of 3×10^{10} Am^{-2}, the field-like term variation is 19.7%, and the damping-like term variation is 16.9% when $H_{x-\mathrm{ext}}$ increases from 250 Oe to 650 Oe. At the current density of 10^{11} Am^{-2}, the field-like term variation increases to 21.5% and the damping-like term variation decrease to 12.4%. The variations are not only the functions of the magnetization uniformity but also the applied current. The role of the current in the variation indicates that possible thermal effect, such as the anomalous Nernst effect, should exist during the SOT measurement[23–26]. In the Ta/Co/Pt stack where our measurements were carried out, there are differences in the resistivity of Ta and Pt. Due to Joule heating which is induced by electric current, the different resistances give rise to a thermal gradient along the normal direction of the stack. The thermal gradient contributes to the measured second harmonic Hall resistances which were used to calculate the SOT effective fields[13]. Depending on the direction of the thermal gradient; the thermal contribution may lead to an over or underestimation of the SOT effective field when the current density increases. However, in our measurement regime, the thermal effects are considered negligible because the current density in our experiments was in the range of ~10^7 A/m^2, where Joule heating is generally negligible[5]. Furthermore, both the damping like term and field like term relates monotonically with the applied current density as shown in Fig. 2, implying that the thermal effects insignificantly to the SOT effective field[27,28].

The magnetization uniformity is equivalent to magnetization amplitude M for the magnetic wire. This magnetization amplitude can be characterized with respect to the applied longitudinal field by measuring $R_{1\mathrm{st\ Hall}}$, thereby obtaining the R_{PHE}. As shown in Fig. 1(b), R_{PHE} increases with respect to $H_{x-\mathrm{ext}}$, where $H_{x-\mathrm{ext}}$ is extended to 100 Oe. This increase is attributed to the polycrystalline structure of the Co layer in the sputtered Ta/Co/Pt film. Without applying $H_{x-\mathrm{ext}}$, the magnetic moment of Co crystalline grains orientates randomly in the film. This is due to the random orientation of the effective field H_{crys} generated by the crystalline magnetic anisotropy of each grain. Hence, the M of the wire equals the value of remanence magnetization M_r, which is determined by the intrinsic demagnetizing field transverse to the wire.

However, when $H_{x-\mathrm{ext}}$ is applied, the magnetic moment **m** of the grains re-orientates towards the x-axis, as schematically shown in Fig. 3(a). Consequently, M increases starting from M_r. The increase of M leads to the

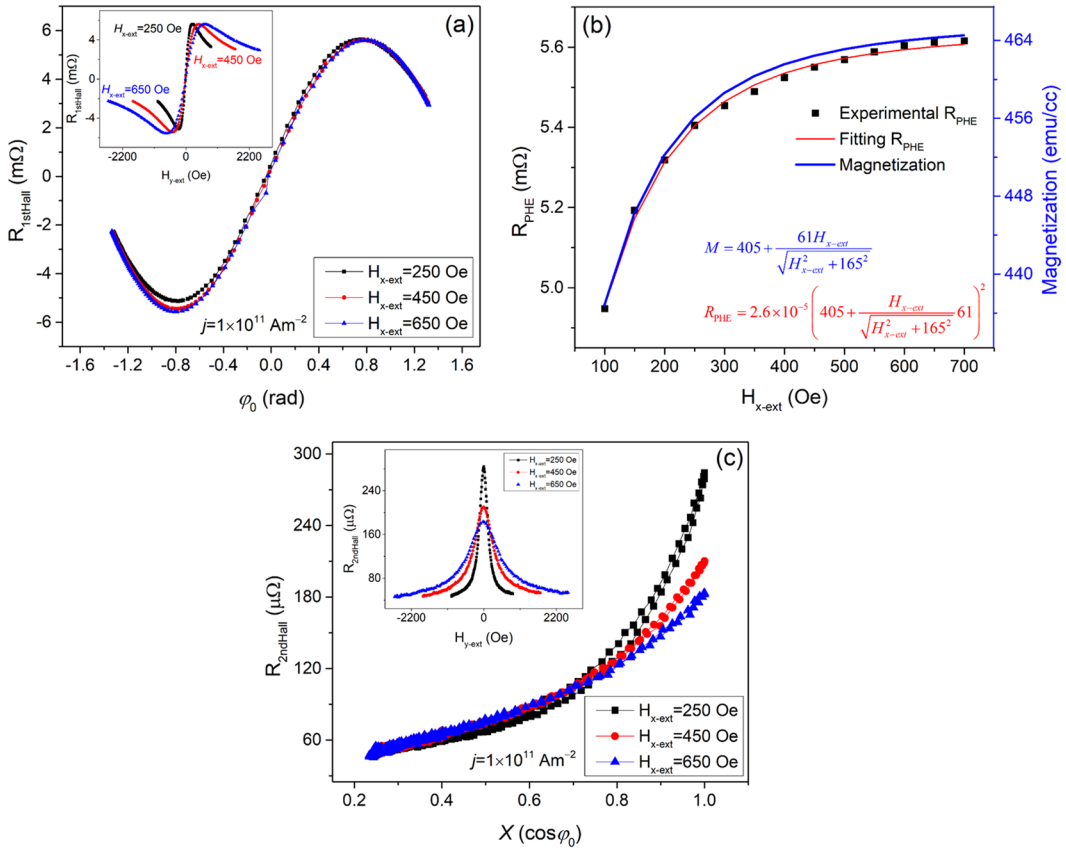

Figure 1. (**a**) The measured first harmonic resistances $R_{1st\,Hall}$ with respect to the azimuthal angle φ_0 of magnetization. Inset is the measured $R_{1st\,Hall}$ with respect to the applied transverse field H_{y-ext}. (**b**) The measured R_{PHE} and the calculated M, with respect to the longitudinal field. R_{PHE} is obtained by fitting the sin2φ_0 curves of (**a**). (**c**) The measured second harmonic Hall resistances $R_{2ndHall}$ with respect to the cosine X of the azimuthal angle. Inset is the measured $R_{2ndHall}$ with respect to applied transverse field H_{y-ext}.

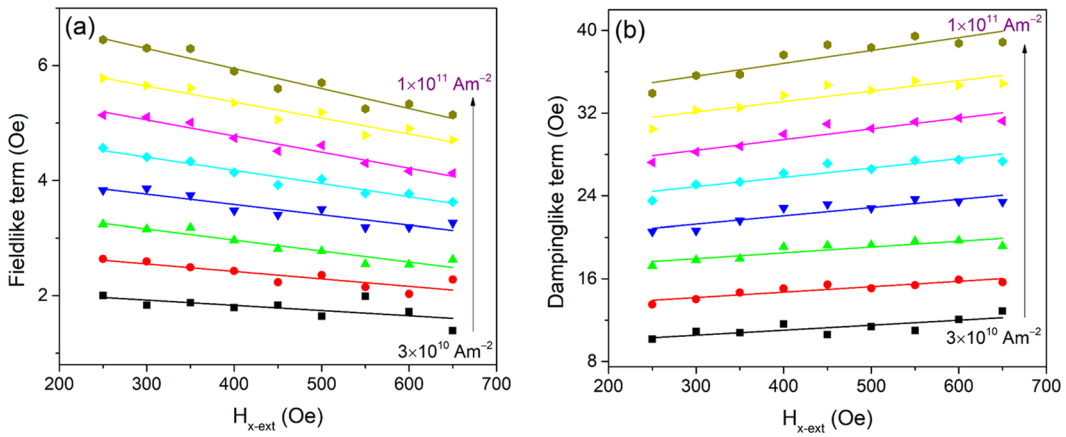

Figure 2. The measured field-like term (**a**), and damping-like term (**b**), with respect to the longitudinal field.

increase of R_{PHE}, as M is related to R_{PHE} by the expression $R_{PHE} = kM^2$ [29–31], where k is a material related coefficient. The maximum of M is the saturation magnetization M_s. Therefore, M_H, defined as $M_H = M_s - M_r$, is the maximum of the magnetization component, which can be manipulated by the external field H_{x-ext}. We consider the magnetization component as the resultant of two vectors expressed by $M_H/2$, instead of evaluating the contribution from each magnetic grain to the magnetization component. As shown in Fig. 3(b), H_{x-ext} orientates both vectors along the x-axis, while the nonzero y component $H_{T,crys}$ of H_{crys} orientates each vector along the $\pm y$ direction, respectively. Hence, each $M_H/2$ orientates at their balanced direction determined by H_{x-ext} and $H_{T,crys}$, as shown in Fig. 3(b). The y components of the two vectors cancel each other, while the x component of each vector

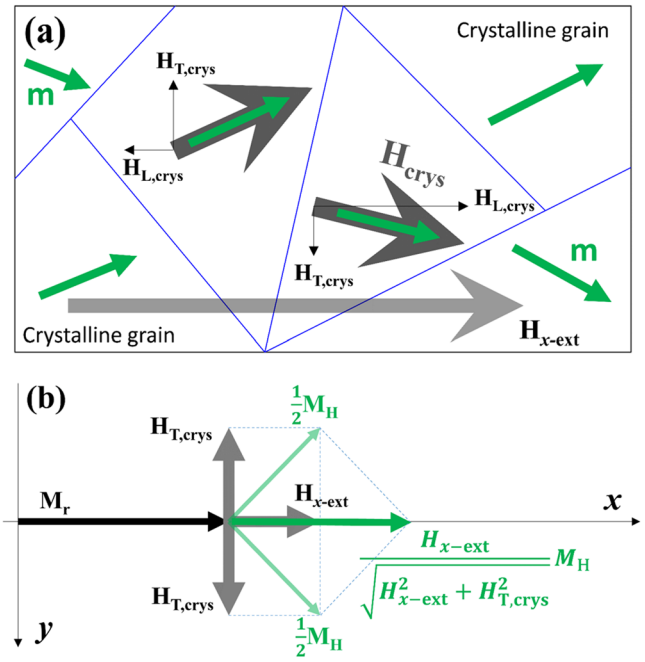

Figure 3. (**a**) The schematic of a polycrystalline magnetic structure and the orientation of magnetic moment for each of crystalline grain under $H_{x-\text{ext}}$ and transverse demagnetizing field. (**b**) The schematic of the magnetization composition for the magnetic structure.

contributes to the magnetization component as $(H_{x-ext}/\sqrt{H_{x-ext}^2 + H_{T,crys}^2})(M_H/2)$. Consequently, the expression of the magnetization component is obtained as $\left(H_{x-ext}/\sqrt{H_{x-ext}^2 + H_{T,crys}^2}\right)(M_H/2)$. Therefore, the total magnetization M can be expressed as $M = M_R + (H_{x-ext}/\sqrt{H_{x-ext}^2 + H_{T,crys}^2})M_H$, and $M_r + M_H$ equals to the saturation magnetization M_s of the wires. Considering $M_r + M_H = 466$ emu/cc for the sample of Ta (4 nm)/Co (2 nm)/Pt (5 nm)[20], and substituting the M expression into the R_{PHE} expression, we fit the measured R_{PHE} as shown in Fig. 1(b). The fitting plot of R_{PHE} matches the experimental R_{PHE}, which verifies the analytical expression of M and gives $M = 405 + (H_{x-ext}/\sqrt{H_{x-ext}^2 + 165^2})61$ emu/cc.

The SOT effective fields per 10^{11} Am^{-2} at each value of $H_{x-\text{ext}}$ were obtained from Fig. 2, for comparison. Replacing $H_{x-\text{ext}}$ with the corresponding value of M shown in Fig. 1(b), the SOT effective fields per 10^{11} Am^{-2} with respect to M are plotted for sample Ta (4 nm)/Co (2 nm)/Pt (5 nm) in Fig. 4. Similarly, the SOT effective fields per 10^{11} Am^{-2} and the magnetization were quantified for samples Ta (t nm)/Co (2 nm)/Pt (5 nm), where $t = 6$, 8 and 10. As reported previously[20], similar saturation magnetization values for the samples $t_{Ta} = 4$ nm and $t_{Ta} = 8$ nm leads to similar tendencies of the field like and damping like fields due to their dependence on magnetization. While substantial differences in the saturation magnetization values for samples $t_{Ta} = 6$ nm and $t_{Ta} = 8$ nm leads to different tendencies of the field-like and damping like SOT fields. As shown in Fig. 4(a,b), the field-like term decreases with respect to the magnetization magnitude while the damping-like term increases in each sample.

We demonstrate that the dependence of the SOT effective fields on the magnetization magnitude or uniformity is attributed to SHE in the Ta/Co/Pt structure. SHE-induced spin accumulation, **s**, which is at the interfaces of Ta/Co and Co/Pt, diffuses into the FM layer to cause STT on the magnetization[9]. In the STT model proposed by S. Zhang[32], the spin current, which is from a reference layer, leads to transverse spin accumulation in the free layer. Consequently, the transverse spin accumulation induces two effective fields: $b\mathbf{m}_r$ and $a\mathbf{m}_f \times \mathbf{m}_r$, where $\mathbf{m}_r$ and $\mathbf{m}_f$ are unit vectors of the local magnetization of the reference layer and the free layer, respectively. When $\mathbf{m}_r$ and $\mathbf{m}_f$ are in the planes of the magnetic layers, b and a are expressed as $b = (hj_e/eM_st_F)\sin\xi.\ e^{-\xi}$ and $a = (hj_e/eM_st_F)(1 - \cos\xi.\ e^{-\xi})$, respectively, where h is the Planck constant, j_e is the electric current density perpendicular to the plane of magnetic layers, t_F is the thickness of the free layer, and e is the electron charge. In the expressions of a and b, ξ equals to $t_F/\sqrt{2}\,\lambda$ with a spin diffusion length $\lambda_f = \sqrt{2hD_0/J}$, where J is a coefficient of the contact interaction between the spin accumulation and the local magnetization of the free layer, and D_0 is the electron diffusion constant. Analogously in the Ta/Co/Pt structure, the Ta or Pt layer is used to generate spin current normal to the magnetic Co layer. Hence, the Ta or Pt layer is similar to the reference layer, as such, **s** can be considered as $\mathbf{m}_r$. The spins generated by the Ta and Pt layers are accumulated at the Co layer, which allows us to take the Co layer as analogous to the free layer. Similarly, **m** is to $\mathbf{m}_f$. Consequently, the field-like term, H_F is equivalent to $b\boldsymbol{m}_r$, and the damping-like term, H_D is equivalent to $a\mathbf{m}_f \times \mathbf{m}_r$. Thus, we obtain $H_F = (hj_e/eM_st_f)(\sin\xi.\ e^{-\xi})$ and $H_D = (hJ_e/eM_st_F)(1 - \cos\xi.e^{-\xi})$ for the Ta/Co/Pt samples, where J_e is the charge current.

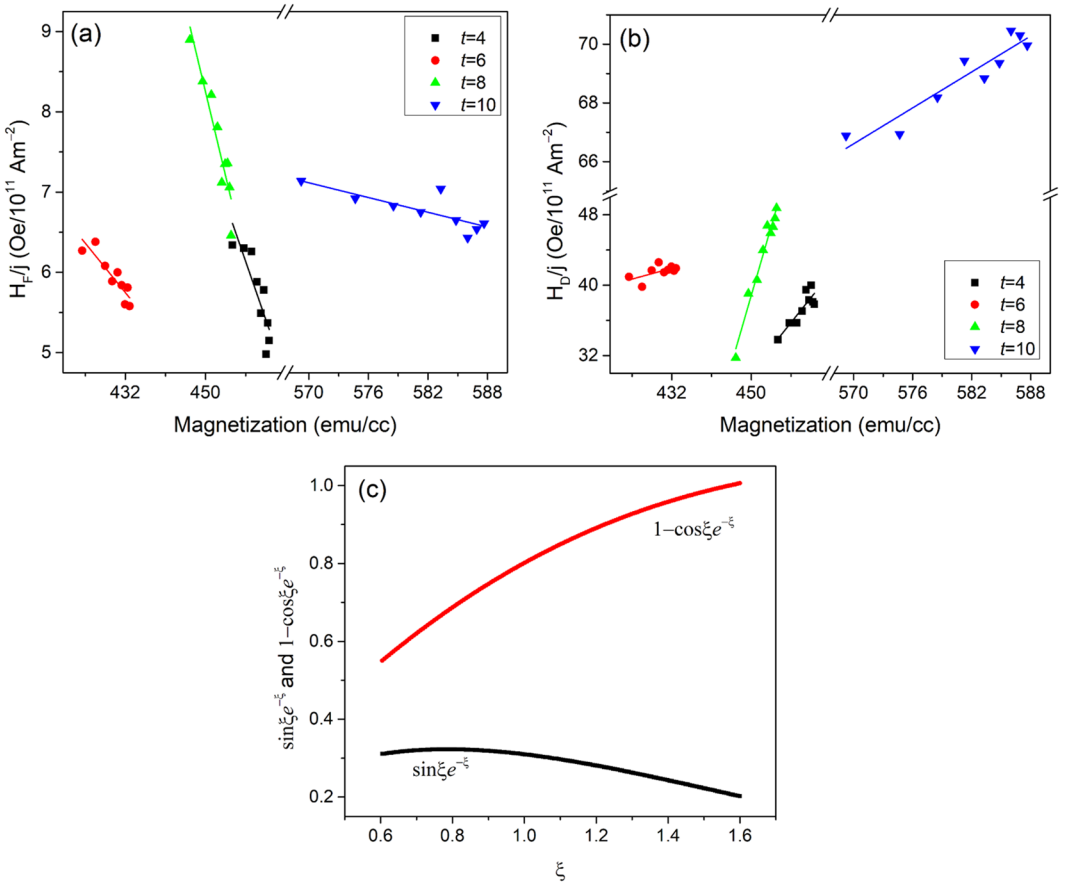

Figure 4. The measured field-like term per current density (**a**), and damping-like term per current density (**b**), with respect to the calculated magnetization M for Ta(t nm)/Co(2 nm)/Pt(5 nm), where $t = 4$, 6, 8 and 10. (**c**) The plots of $\sin\xi e^{-\xi}$ and $1-\cos\xi e^{-\xi}$ with respect to ξ.

We propose that the magnetization magnitude of Co layer manipulate the SOT effective fields *via* the coefficient ξ, considering the above expressions of H_F and H_D. The damping-like term is related to spin Hall angle θ_{SH} *via* the expression $H_D = \theta_{SH} h j_e / e M_s t_F$, where θ_{SH} is defined as the ratio of spin current j_s to charge current j_e[19,33–35]. Comparing the two expressions of H_D, we obtain $\theta_{SH} = 1 - \cos\xi e^{-\xi}$ As such, ξ is ≤ 1.6, since the sum of Pt and Ta spin Hall angles is ≤ 1[7,36]. As $\xi = t_F/(\sqrt{2}\lambda_J)$ and λ_J is about 1.2~2.4 nm for Co[25], we obtain $\xi \geq 0.6$, using the Co layer thickness $t_F = 2$ nm. Therefore, our samples have values of $0.6 \leq \xi \leq 1.6$. ξ can be rewritten as $\xi = (t_F/2)\sqrt{J/hD_0}$, where D_0 is related to the magnetization of the wire[30,37]. Ustinov created a superlattice model to explain the correlation of D_0-related magnetoresistance (MR) and magnetization[37]. In this model, the superlattice comprises of several magnetic layers, and for any of two adjacent layers, magnetizations are initially antiparallel to each other. A transverse magnetic field, which is perpendicular to the initial magnetization in the plane of the magnetic layers, is applied to change the magnetization amplitude of the superlattice. The model concludes that the MR increases with respect to the magnetization of the superlattice. Hence, D_0 decreases with increasing magnetization in our samples, as it is inverse proportional to MR. Therefore, ξ increases with respect to the magnetization magnitude, due to $\xi = (t_F/2)(/)(\sqrt{J/hD_0})$. In the range of 0.6~1.6 for our samples, the increase of ξ leads to the decrease of the term $\sin\xi e^{-\xi}$ and increase of the term $1-\cos\xi e^{-\xi}$, as shown in Fig. 4(c). Therefore, H_F decreases and H_D increases with respect to the magnetization, respectively, as the term $hj_e/eM_s t_F$ is a constant for each sample.

Conclusion

In conclusion, our measurement results show that the SOT effective fields depend on the magnetization uniformity in Ta/Co/Pt structure. The dependence indicates that the SOT effective fields can be manipulated by varying the magnetization uniformity. The change of magnetization uniformity was achieved in each sample by applying magnetic fields along the long axis of the wire. As the SOT effective fields are concurrently characterized, our characterization method eliminates influences from other SOT dependence effects. As an analogy to the STT effect from a reference layer, the SOT dependence on the magnetization uniformity is attributed to the electron diffusion properties. This dependence suggests that SHE plays a significant role in the dependence of SOT effective fields on magnetization. It also indicates that the SOT effective fields cannot be considered as constant

parameters when analyzing domain wall dynamics *via* SOT. Moreover, we conclude that magnetization enhances the damping-like torque while suppressing the field-like torque.

References

1. Parkin, S. S. P., Hayashi, M. & Thomas, L. Magnetic domain-wall racetrack memory. *Science (New York, N.Y.)* **320**, 190–4 (2008).
2. Ralph, D. C. & Stiles, M. D. Spin transfer torques. *Journal of Magnetism and Magnetic Materials* **320**, 1190–1216 (2008).
3. Emori, S., Bauer, U., Ahn, S. M., Martinez, E. & Beach, G. S. D. Current-driven dynamics of chiral ferromagnetic domain walls. *Nature Materials* **12**, 611–616 (2013).
4. Ryu, K.-S., Thomas, L., Yang, S.-H. & Parkin, S. Chiral spin torque at magnetic domain walls. Supplementary Information. *Nature nanotechnology* **8**, 527–33 (2013).
5. Pi, U. H. *et al*. Tilting of the spin orientation induced by Rashba effect in ferromagnetic metal layer. *Applied Physics Letters* **97**, 162507 (2010).
6. Hayashi, M., Kim, J., Yamanouchi, M. & Ohno, H. Quantitative characterization of the spin-orbit torque using harmonic Hall voltage measurements. *Physical Review B - Condensed Matter and Materials Physics* **89**, 144425 (2014).
7. Woo, S., Mann, M., Tan, A. J., Caretta, L. & Beach, G. S. D. Enhanced spin-orbit torques in Pt/Co/Ta heterostructures. *Applied Physics Letters* **105**, 212404 (2014).
8. Manchon, A. & Zhang, S. Theory of nonequilibrium intrinsic spin torque in a single nanomagnet. *Physical Review B* **78**, 212405 (2008).
9. Skinner, T. D. *et al*. Complementary spin-Hall and inverse spin-galvanic effect torques in a ferromagnet/semiconductor bilayer. *Nature Communications* **6**, 6730 (2015).
10. Wong, Q. Y. *et al*. Enhanced Spin-Orbit Torques in Rare-Earth Pt/$[Co/Ni]_2$/Co/Tb. *Physical Review Applied* **11**, 024057 (2019).
11. Hayashi, M. *et al*. Domain wall dynamics driven by spin transfer torque and the spin–orbit field. *Journal of Physics: Condensed Matter* **24**, 024221 (2011).
12. Garello, K. *et al*. Symmetry and magnitude of spin–orbit torques in ferromagnetic heterostructures. *Nature Nanotechnology* **8**, 587–593 (2013).
13. Avci, C. O. *et al*. Fieldlike and antidamping spin-orbit torques in as-grown and annealed Ta/CoFeB/MgO layers. *Physical Review B* **89**, 214419 (2014).
14. Lee, H. R. *et al*. Spin-orbit torque in a bulk perpendicular magnetic anisotropy Pd/FePd/MgO system. *Scientific Reports* **4**, 6548 (2014).
15. Qiu, X. *et al*. Angular and temperature dependence of current induced spin-orbit effective fields in Ta/CoFeB/MgO nanowires. *Scientific Reports* **4**, 4491 (2014).
16. Lee, K. S. *et al*. Angular dependence of spin-orbit spin-transfer torques. *Physical Review B - Condensed Matter and Materials Physics* **91**, 144401 (2015).
17. Wong, Q. Y. *et al*. *In situ* Kerr and harmonic measurement in determining current-induced effective fields in MgO/CoFeB/Ta. *Journal of Physics D: Applied Physics* **51**, 115004 (2018).
18. Kim, J. *et al*. Layer thickness dependence of the current-induced effective field vector in Ta|CoFeB|MgO. *Nature Materials* **12**, 240–245 (2012).
19. Fukami, S., Anekawa, T., Zhang, C. & Ohno, H. A spin-orbit torque switching scheme with collinear magnetic easy axis and current configuration. *Nature Nanotechnology* **11**, 621–625 (2016).
20. Luo, F. *et al* Simultaneous determination of effective spin-orbit torque fields in magnetic structures with in-plane anisotropy. *Physical Review B* **95** (2017).
21. Engel, C., Goolaup, S., Luo, F. & Lew, W. S. Quantitative characterization of spin-orbit torques in Pt/Co/Pt/Co/Ta/BTO heterostructures due to the magnetization azimuthal angle dependence. *Physical Review B* **96**, 54407 (2017).
22. Li, S. *et al*. Deterministic Spin-Orbit Torque Induced Magnetization Reversal in Pt/[Co/Ni] n /Co/Ta Multilayer Hall Bars. *Scientific Reports* **7**, 972 (2017).
23. Wang, W. G., Chien, C. L., Huang, S. Y., Lee, S. F. & Kwo, J. Intrinsic Spin-Dependent Thermal Transport. *Physical Review Letters* **107**, 216604 (2011).
24. Kikkawa, T. *et al*. Longitudinal spin seebeck effect free from the proximity nernst effect. *Physical Review Letters* **110**, 67207 (2013).
25. Schmid, M. *et al*. Transverse Spin Seebeck Effect versus Anomalous and Planar Nernst Effects in Permalloy Thin Films. *Physical Review Letters* **111**, 187201 (2013).
26. Bauer, G. E. W. Spin caloritronics. *Spin Current* **11**, 143–159 (2017).
27. Ueda, K., Pai, C. F., Tan, A. J., Mann, M. & Beach, G. S. D. Effect of rare earth metal on the spin-orbit torque in magnetic heterostructures. *Applied Physics Letters* **108**, 232405 (2016).
28. Meng, K. *et al*. Modulated switching current density and spin-orbit torques in MnGa/Ta films with inserting ferromagnetic layers. *Scientific Reports* **6**, 1–8 (2016).
29. Ky, V. D. & N, I. A. 2-Dimension galvanomagnetic effect in thin ferromagnetic films. *Ser. Fiz.* **29**, 576 (1965).
30. Ky, V. D. Planar Hall Effect in Ferromagnetic Films. *Physica Status Solidi (B)* **26**, 565–569 (1968).
31. Yu, M. L. & Chang, J. T. H. The temperature dependence of the planar hall effect in iron, cobalt and nickel. *Journal of Physics and Chemistry of Solids* **31**, 1997–2002 (1970).
32. Zhang, S., Levy, P. M. & Fert, A. Mechanisms of spin-polarized current-driven magnetization switching. *Physical Review Letters* **88**, 2366011–2366014 (2002).
33. Fan, X. *et al*. Quantifying interface and bulk contributions to spin-orbit torque in magnetic bilayers. *Nature Communications* **5**, 3042 (2014).
34. Seo, S. M., Kim, K. W., Ryu, J., Lee, H. W. & Lee, K. J. Current-induced motion of a transverse magnetic domain wall in the presence of spin Hall effect. *Applied Physics Letters* **101** (2012).
35. Khvalkovskiy, A. V., *et al* Matching domain-wall configuration and spin-orbit torques for efficient domain-wall motion. *Physical Review B* **87,**020402(R) (2013).
36. Hoffmann, A. Spin hall effects in metals. *IEEE Transactions on Magnetics* **49**, 5172–5193 (2013).
37. Ustinov, V. V. & Kravtsov, E. A. A unified semiclassical theory of parallel and perpendicular giant magnetoresistance in metallic superlattices. *Journal of Physics: Condensed Matter* **7**, 3471–3484 (1995).

Acknowledgements

This work was supported by the Singapore National Research Foundation, Prime Minister's Office, under a Competitive Research Programme (Non-volatile Magnetic Logic and Memory Integrated Circuit Devices, NRF-CRP9-2011-01), and an Industry-IHL Partnership Program (NRF2015-IIP001-001). The supports from a RIE2020 ASTAR AME IAF-ICP Grant (No.I1801E0030) and an ASTAR AME Programmatic Grant (No. A1687b0033) are also acknowledged. WSL is a member of the SG-SPIN Consortium. The authors acknowledge Sarjoosing Goolaup and Christian Engel for fruitful discussions related to this work.

Author Contributions

F.L. Luo carried out the experiments. S.H. Li, F.N. Tan, and G.J. Lim assisted in the thin film deposition and electron beam patterning. F.L. Luo, Q.Y. Wong, and W.S. Lew prepared the figures and the main manuscript. All authors discussed the data and the results and commented on the manuscript. W.S. Lew supervised the project.

Additional Information

Competing Interests: The authors declare no competing interests.

Publisher's note: Springer Nature remains neutral with regard to jurisdictional claims in published maps and institutional affiliations.